Peer-reviewed version available at *Catalysts* **2020**, *10*, 138; doi:10.3390/catal10010138

Article

Rapid Removal of Azophloxine via Catalytic Degradation by A Novel Heterogeneous Catalyst under Visible Light

Di Wu, Kequan Xia, Chengzhu Fang, Xue-Gang Chen* and Ying Ye

Ocean College, Zhejiang University, Zhoushan, 316021 P.R. China

*To whom correspondence should be addressed: Xue-Gang Chen, email: chenxg83@zju.edu.cn; Tel: +86-580-2092326, Fax: +86-580-2092891.

Abstract: Azo dyes are the most widely used synthetic dyes in the printing and dyeing process. However, the discharge of untreated azo dyes poses a potential threat to the aqueous ecosystem and human health. Herein, we fabricated a novel heterogeneous catalyst - activated carbon fiber-supported ferric alginate (FeAlg-ACF). Together with peroxymonosulfate (PMS) and visible light, this photocatalytic oxidation system was used to remove an azo dye - azophloxine. The results indicated that the proposed catalytic oxidation system can remove 100% azophloxine within 24 min, while under the same system, the removal rate was only 92 % and 84 % when ferric alginate was replaced with ferric citrate and ferric oxalate respectively, which showed the superiority of FeAlg-ACF. The degradation of azophloxine is achieved by the active radicals ($SO_4^{\bullet-}$ and •OH) released from PMS and persistent free radicals from activated carbon fiber. Moreover, due to ferric alginate 's highly intrinsic photosensitivity, visible radiation can further enhance the LMCT processes. After treating for 24 min, the total organic carbon of azophloxine solution (50 μmol/L) decreased from 1.82 mg/L to 79.3 μg/L and the concentration of nitrate ions increased from 0.3 mg/L to 8.6 mg/L. That is, up to 93.5% of azophloxine molecules were completely degraded into inorganic compounds. Consequently, potential secondary contamination by intermediate organic products during catalytic degradation was prohibited. The azophloxine removal ratio was kept almost constant after seven cycles, indicating the recyclability and longevity of this system. Furthermore, the azophloxine removal was still promising at high concentrations of Cl^-, HCO_3^-, CO_3^{2-}. Therefore, our proposed system is potentially effective to remove dye pollutants from seawater. It provides a feasible method for the development of efficient and environmental friendly PMS activation technology combined with FeAlg-ACF, has significant academic and application value.

Keywords: peroxymonosulfate; ferric alginate; activated carbon fiber; visible radiation; heterogeneous photocatalysis

1. Introduction

Azo dyes are widely used in printing and dyeing industries. However, about 10% - 15% of residual azo dyes are discharged into the environment without treatment, which poses severe environmental pollution and hazard for aqueous organisms and human health [1-4]. Therefore, it is of great practical significance to develop efficient and environmentally friendly treatment methods for dyeing wastewater. Among many water pollution treatment methods, Fenton-like oxidation technology, as a typical advanced oxidation technology, has been widely favored by researchers due to its advantages of high efficiency, environmental friendliness, and circularity [5-9]. The amount of reactive oxygen species (ROS) is an important factor for the catalytic efficiency of the photocatalytic system, especially in relatively mild conditions [10-13]. Peroxymonosulfate (PMS) is a widely used material to provide ROS to remove a variety of refractory organic pollutants in environmental remediation[14,15]. PMS could be activated to produce •OH and $SO_4^{\bullet-}$ by transition metal ions with advantages of simple reaction conditions, rapid reaction rate, and low cost [16-18].

Studies have shown that Fe(III) is easy to form complexes with carboxyl groups [19-22]. These complexes are often photoactive and can be decomposed under the light to produce a variety of active species (Eqs. (1) – (7)):

$$RCOO\text{-}Fe(III) + hv \rightarrow Fe(II) + RCOO- \quad (1)$$

$$RCOO\bullet \rightarrow R\bullet + CO_2 \quad (2)$$

$$R\bullet + Fe(II) \rightarrow Fe(III) + products \quad (3)$$

$$R\bullet + O_2 \rightarrow O_2^{-}\bullet + products \quad (4)$$

$$H^+ + O_2^{-}\bullet \rightarrow HO_2\bullet \quad (5)$$

$$HO_2\bullet + HO_2\bullet \rightarrow H_2O_2 + O_2 \quad (6)$$

$$HO_2\bullet + H^+ + Fe(II) \rightarrow H_2O_2 + Fe(III) \quad (7)$$

In analogy to other Fe(III)-carboxylate complexes, such as ferric citrate and ferric oxalate [23–25], ferric alginate (Fe-Alg) could initiate the generation of a series of active oxygen species and Fe(II)/Fe(III) ions by the photo-induced ligand-metal electron transfer (LMCT) under light irradiation [26]. However, ferric citrate and ferric oxalate are greatly affected by the pH value. When the pH value is greater than 4, both the ferric citrate and ferric oxalate complex will be converted into $Fe_2O_3\bullet nH_2O$ amorphous precipitation, leading to the decrease or disappearance of the optical activity of the system [27].

As an iron-based photocatalyst, Fe-Alg complex is made by cross-linking the multivalent Fe(III) with natural, non-hazardous and edible polysaccharide alginate [28]. There are a large number of carboxyl groups in the molecular structure of alginate. Studies have shown that some carboxyl acids can produce active reducing free radicals by self-photolysis, and there are also a large number of hydroxyl groups. Thanks to the unique gelling properties, alginates can react with metal ions to form stable organic-inorganic hybrid composite materials, which may be found promising applications in the environmental purification and remedy areas [29-33].

Although iron alginate gel beads have been studied that can increase the pH range of Fenton-like catalysts in recent years [34], it still has some unresolved difficulties, such as tedious preparation process, non-reuse, hydrolysis under a strong base [35-37]. Therefore, it is necessary to construct a heterogeneous catalytic system with Fe-Alg as the active center to accelerate the process of metal-ligand-charge transfer and improve the stability of materials, so as to improve the degradation efficiency of dye wastewater.

The suitable carrier is also essentially important for a catalytic system. The commonly used heterogeneous catalytic carriers are zeolite, resin, clay, molecular sieve, activated carbon, etc [38-41]. Among them, activated carbon has attracted extensive attention due to its large specific surface area and strong adsorption performance. However, activated carbon is generally powdered or granular, and there are still problems such as separation and regeneration difficulties between catalyst and reaction medium. Compared with powdered or granular activated carbon, activated carbon fiber has more excellent properties [42]. Due to its microporous structure, ACF usually shows a specific surface area of up to 3000 m^2/g with an average value of 1000 - 1500 m^2/g [43-45]. The outer surface area of ACF is two orders of magnitude higher than the internal surface area. Therefore, ACF could provide high adsorption efficiency for the photocatalytic system. The adsorption ability of ACF is stronger than that of activated carbon for some macromolecules or particles [46,47]. Furthermore, the surface of ACF contains abundant oxygen-bearing groups, and its surface structure can be modified to further improve its adsorption performance [48,49]. On the other hand, ACF could provide large amounts of persistent free radicals (PFRs) for the metal-ligand Fe, which helps to further accelerate the LMCT process and reduce Fe(III) to Fe(Il) state [15,50]. Therefore, when transition metals such as Fe, Cu, Co, and Ni are loaded on the surface of ACF, through ACF inherent PFRs start the electron transfer in catalytic oxidation and continue to provide electron, those transition metals can accelerate high transition metal reduction reaction with visible light photocatalytic synergy, activate the PMS to produce ROS, thus degrade organic dyes.

In this work, we reported a novel photocatalytic oxidation system (FeAlg-ACF/PMS/visible light) for the first time. The ACF served as the carrier, and PMS provided oxidants, Fe-Alg were

Peer-reviewed version available at Catalysts 2020, 10, 138; doi:10.3390/catal10010138

loaded on the surface of ACF via a simple impregnation method to create a Fenton-like catalyst FeAlg-ACF. We assessed the removal of azo dyes by this novel system and investigated the optimum treating conditions. In addition, we proposed the potential degradation mechanism of azo dyes by FeAlg-ACF/PMS under visible light.

2. Results and discussions

2.1. Characteristics of the as-prepared catalyst

Surface topography of ACF and FeAlg-ACF were evaluated by SEM. Fig. 1 (a) and (c) respectively showed the surface morphologies of ACF and FeAlg-ACF at 5000 times. The iron alginate was densely and uniformly distributed on the surface of ACF. In addition, the iron content of the precipitated solution after the formation of the heterogeneous catalyst FeAlg-ACF was texted for only 0.026% by XRF. It was indicated that iron had been successfully loaded onto ACF. The microscopy results suggested that Fe-Alg particles were densely and uniformly cross-linked distributed on the surface of ACF. At high magnification, as shown in Fig 1 (b) and (d), the loaded Fe-Alg particles showed rod-like shapes with a width of about 40 nm and a length of 60 nm.

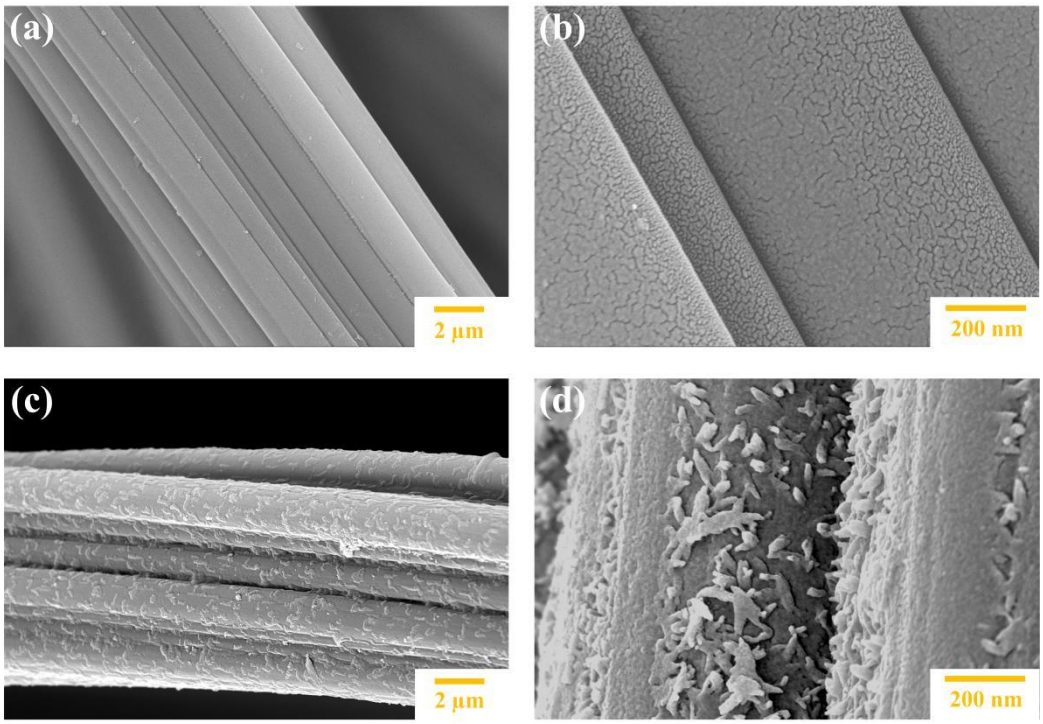

Figure 1. SEM image of: ACF at magnification of 5000 (a) and 45000 (b) as well as the FeAlg-ACF catalyst at magnification of 5000 (c) and 45000 (d).

2.2. Dye removal by Fe-Alg catalyst

The removal of azophloxine by different systems were investigated in dark and visible light. As shown in Fig. 2A, ACF and FeAlg-ACF removed 8% and 10% of azophloxine respectively after 24 min in dark condition, suggesting that the adsorption of azophloxine by ACF and FeAlg-ACF was quite limited. The adsorption equilibrium achieved after 12 min. By contrast, when PMS was introduced, about 47% of azophloxine was removed by the Fe-Alg/PMS system. It indicated that PMS can significantly improve the removal of dyes because of its activation by Fe-Alg to generate $SO_4^{\bullet-}$ efficiently. Surprisingly, when the FeAlg-ACF/PMS system was exposed to visible radiation, almost all the azophloxine was rapidly removed from the solution within 24 min. Correspondingly, the characteristic absorption peak of azophloxine at 531 nm gradually decreased with time, and totally disappeared after 24 min (Fig. 2C). The result suggested that azophloxine had been degraded rapidly by the FeAlg-ACF/PMS system under visible light irradiation, testified by the decreasing of total

organic carbon content from 1.82 mg/L to 79 μg/L. In addition, the nitrate (NO_3^-) concentration increased from 0.3 mg/L before catalytic degradation to 8.6 mg/L after 24 min treatment. According to the molecular structure of azophloxine, the complete degradation of this dye with an initial concentration of 50 μmol/L would generate a nitrate content of 8.6 mg/L in the resulting solution. Consequently, about 93.5% of azophloxine molecules had been completely degraded into inorganic compounds after the treatment of the FeAlg-ACF/PMS system, which paved an avenue for developing high-efficiency processes to be subsequently used in environmental catalysis.

The effects of different systems on azophloxine removal were compared in Fig. 2B. Comparative experiments with ferric alginate (Fe-Alg), ferric citrate (Fe-Cit) and ferric oxalate (Fe-Msds) under the same carrier and oxidant were tested. The results indicated that the proposed catalytic oxidation system can remove 100% azophloxine within 24 min, while under the same system, the removal rates were only 92% and 84% when Fe-Alg was replaced with Fe-Cit and Fe-Msds respectively. It was related to the photosensitivity of Fe-Alg and its unique complexation structure. When ACF reacted with the oxidant PMS alone, the removal rate was 60% after 24 min. This phenomenon is attributed to the fact ACF is a porous carbon material, which can adsorb 8% azophloxine. On the other hand, ACF will continuously provide PFRs as electronic storage to participate in the LMCT process, under the irradiation of light, PMS is activated by electron transfer to produce small amounts of $SO_4^{\bullet-}$ and •OH to degrade dye.

Our prepared FeAlg-ACF/PMS system could sustain several cycles. As shown in Fig. 2D, the removal efficiency of azophloxine after 24 min kept almost constant after seven cycles, decreased slightly from 100% to 93%. It is ascribed to the high structural stability, repeatability and recycling performance of the FeAlg-ACF photocatalyst. Meanwhile, our chosen oxidant PMS is stable during dye treatment, and the treatment process is in line with safety and environmental protection requirements. Furthermore, we also assessed the removal efficiency of our catalytic system for acid orange 7 and methylene blue. The removal ratios of acid orange 7 and methylene blue achieved 98.0% and 97.4% by FeAlg-ACF/PMS under visible light irradiation after 24 min. Our system, therefore, shows great potential for the removal of reactive dyes, acid dyes, and other typical dyes, and is promising to be applied in dye wastewater treatment and environmental restoration.

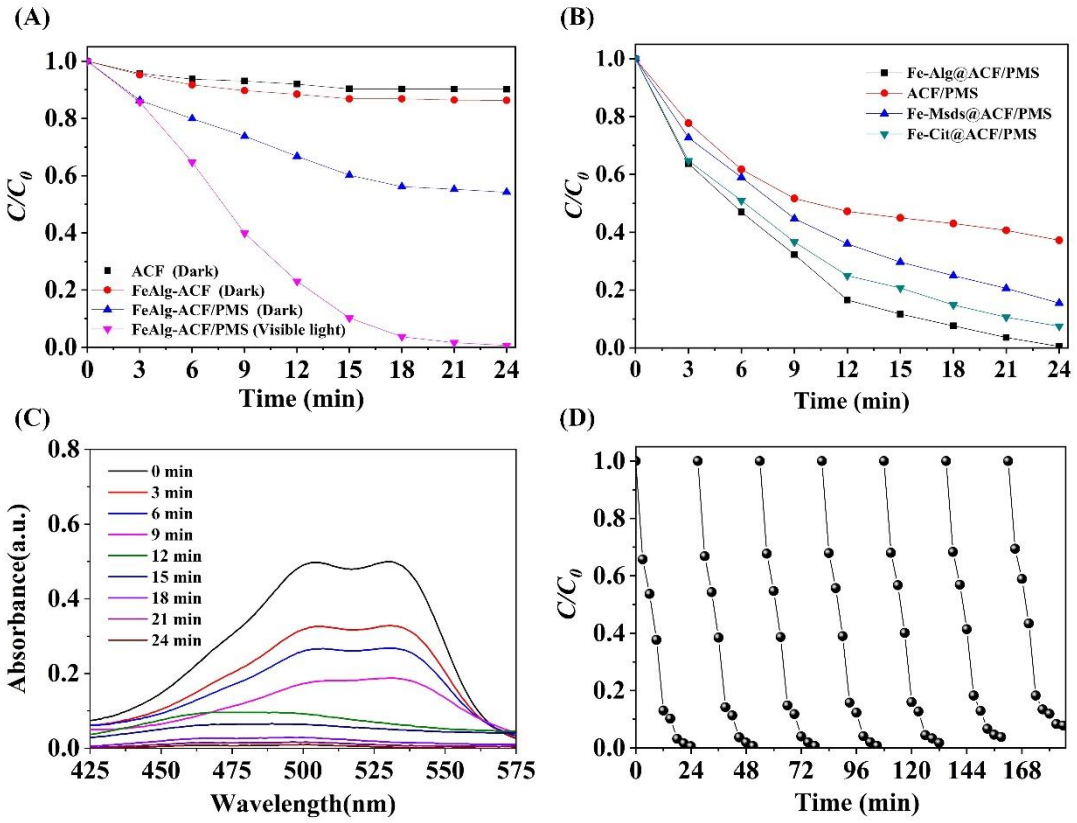

Figure 2. (A) Time-dependent profiles of azophloxine decolorization with and without light irradiation. (B) Decolorization of azophloxine by different systems as a function of time; (C) UV–Vis spectra of azophloxine solutions after removal by FeAlg-ACF/PMS system. (D) Azophloxine removal by FeAlg-ACF/PMS after certain cycles. Reaction conditions: [FeAlg-ACF] = 2 g/L, [PMS] = 5 mmol/L, [azophloxine] = 50 μmol/L, initial pH = 4.0, T = 25 ℃.

2.3. Effect of reaction conditions

2.3.1. Effect of PMS dosage

PMS produces ROS in the reaction system and provides oxidant for the catalytic degradation of organic pollutants by catalyst. The removal ratio of azophloxine in our catalytic system varied with the initial PMS concentration, as shown in Fig. 3A. After 24 min treatment, the removal ratio enhanced from 74% to 100% as the PMS dosage increased from 0 to 5 mmol/L. At the PMS concentration of 5 mmol/L, azophloxine was completely degraded within 9 min when the initial pH was 4. The enhanced removal of azophloxine by increasing PMS concentrations was attributed to the increased generation of ROS which was conducive to the catalytic reaction. In consideration of environmental protection, economy, and practicability, the initial content of PMS was set as 5 mmol/L in the following experiments. Besides, we calculated the utilization efficiency of PMS using the oxidant consumption index (X): the number of azophloxine is removed per mole number of oxidant consumed. A lower X value indicates a higher utilization efficiency of oxidant [54]. We calculated that our catalytic system (X=31.4) showed excellent PMS utilization compared with Fe-Alg/PMS system (X=43.7) and FeAlg-ACF/PMS system (X=57.1) without visible light radiation.

2.3.2. Effect of initial pH values

The influence of initial pH values on azophloxine removal is illustrated in Fig. 3B. More than 95% azophloxine was removed by the FeAlg-ACF/PMS system at pH values of 2.0 - 8.0 within 24 min when other parameters were kept constant. $S_2O_8^{2-}$ ions that produced by PMS after activation can react with water or OH^- to produce •OH. $SO_4^{\bullet-}$ and •OH mainly come from PMS photolysis, $SO_4^{\bullet-}$ decay and transformation of $SO_4^{\bullet-}$ to •OH. When the pH is greater than 7, the ROS in the system is dominated by •OH. When the pH value is 7, $SO_4^{\bullet-}$ is equally involved in oxidation as •OH (Eqs. (8)-(9)).

$$SO_4^{\bullet-} + H_2O \rightarrow SO_4^{2-} + \bullet OH + H^+ \quad (8)$$

$$SO_4^{\bullet-} + OH^- \rightarrow SO_4^{2-} + \bullet OH \quad (9)$$

Compared with the typical Fenton system, our system shows excellent degradation performance under weak alkaline conditions. This is because as the pH value increases, the carboxyl dissociation on alginate is in a state of negative charge, and the pores of the gel structure increase under the action of electrostatic repulsion, so the ability to absorb dye molecules is enhanced. The removal ratio of azophloxine generally decreases with increasing pH values (Fig. 3B). When the initial pH value was 2.0, the time required to completely remove azophloxine was only 12 min, which was quite superior when compared with other photocatalytic Fenton system [55]. At an initial pH value of 10.0, however, the azophloxine removal ratio was significantly declined to only 65 % after 24 min, but there was still a downward trend. This result also indicated that our FeAlg-ACF/PMS could effectively remove azophloxine in a wide pH range of 2 - 10. By contrast, traditional homogeneous or heterogeneous Fenton systems only work in narrow pH ranges (usually 2 - 4) [56,57].

2.3.3. Effect of treating temperature

Temperature is an important factor affecting the process of activating PMS to degrade organic matter. Increasing temperature can not only promote the molecular thermal movement which improves the reaction rate of wastewater treatment but also make the reaction system more easily overcome the reaction activation energy. As shown in Fig. 3C, when the reaction temperature was lower than 30 ℃, the removal of azophloxine increased with augmenting temperature. When the

temperature was higher than 30 ℃, on the contrary, the photocatalytic degradation of azophloxine generally declined with increasing temperature. When the reaction temperature reached 50 ℃, the azophloxine removal ratio was 90% after processing for 27 min. Because room temperature was close to the optimal reaction temperature (30 ℃), the reaction temperature was set at 25 ℃ in the following experiments to facilitate the operation of experiments.

2.3.4. Impact of ion strength

Chloride can promote the transfer of dye from the aqueous phase to the fibrous phase, widely used in the printing and dyeing industry. Besides, there is a mass of chloride, carbanion and bicarbonate ion in the seawater system [58]. Therefore, it is necessary to study the effect of chloride, carbanion and bicarbonate ion on the oxidation activity of the catalytic system.

Fig. 3D shows the change of azophloxine removal rate in our catalytic system under different concentrations of NaCl. As shown in Fig. 3D, when NaCl concentration increased from 0 to 0.05 mmol/L, the removal rate of azophloxine in our catalytic system decreased, which could be attributed to the scavenging effect of •OH in NaCl. In our catalytic system, when NaCl concentration increased from 0.05 mmol/L to 0.1 mmol/L, the azophloxine removal rate increased. When chloride concentration was 0.1 mmol/L, the azophloxine removal rate was the highest, reaching 98% removal rate within 30 minutes. Chloride promoted pollutant removal. However, when NaCl concentration exceeded 0.1 mmol/L, with the further increase of NaCl concentration, azophloxine removal rate decreased, it showed that a high concentration of chloride inhibited azophloxine degradation.

The effect of widespread carbanion (CO_3^{2-}) in seawater on azophloxine degradation was illustrated in Fig. 3E, when the concentration of CO_3^{2-} increased, the removal rate of azophloxine becomed faster, which demonstrated the introduction of CO_3^{2-} promoted the removal of azophloxine. The introduction of HCO_3^- had a slight inhibitory effect on the removal of azophloxine, and with the increase of HCO_3^- concentration, the overall effect of first promoting and then inhibiting appeared, as presented in Fig. 3F. Therefore, we speculate that a low concentration of HCO_3^- is involved in the pathway to promote the generation of •OH and $SO_4^{\bullet -}$, thus promoting the removal of azophloxine, while the excessive concentration of HCO_3^- could capture ROS generated by the reaction to restrain the removal of azophloxine.

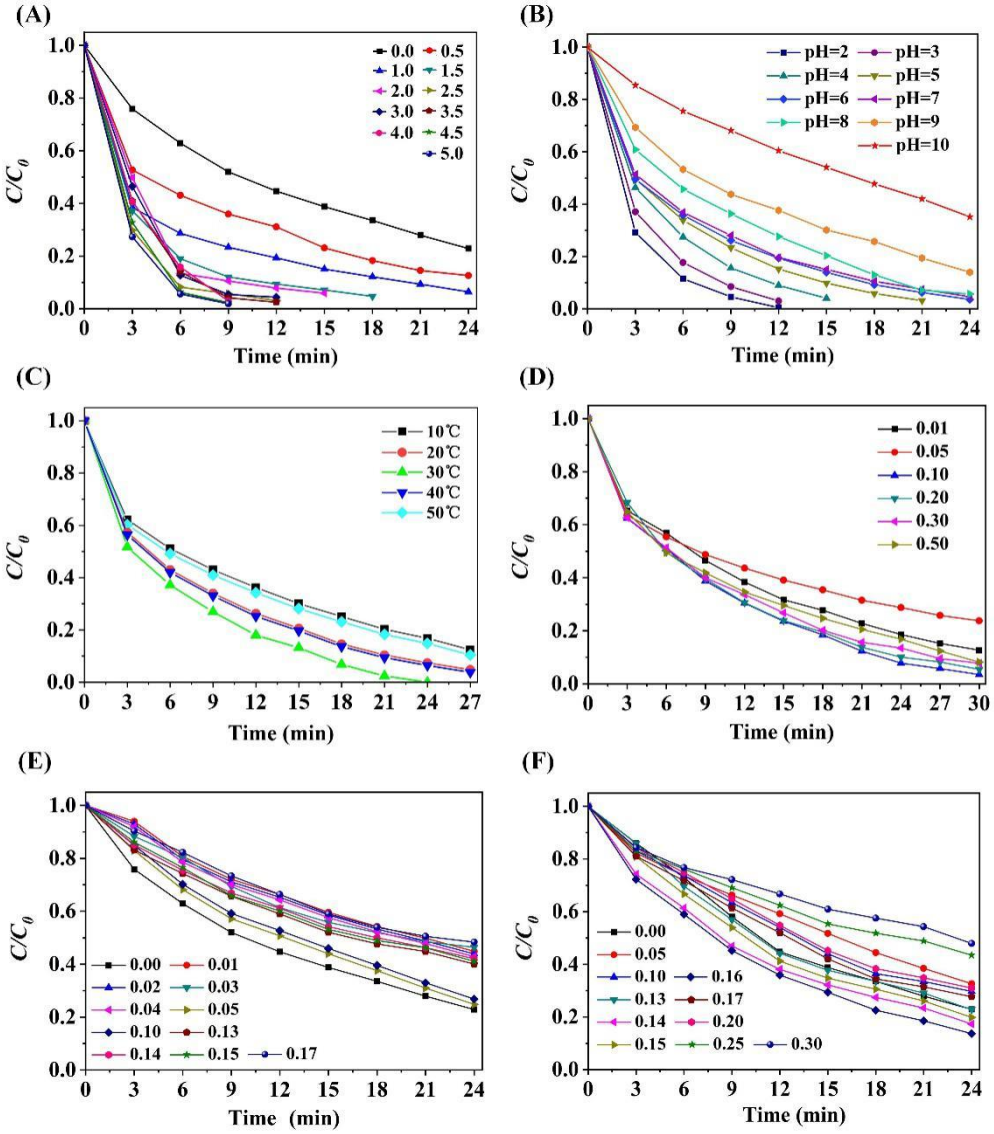

Figure 3. Time-dependent profiles of azophloxine removal under in different conditions: (A) Effect of PMS dosage. Reaction conditions: T = 25 °C, pH = 4. (B) Effect of initial pH. Reaction conditions: [PMS] = 5 mmol/L, T = 25 °C. (C) Effect of reaction temperature. (D) Effect of initial NaCl concentration. Concentration unit: mmol/L (E) Effect of initial Na_2CO_3 concentration. Concentration unit: mmol/L (F) Effect of initial $NaHCO_3$ concentration. Concentration unit: mmol/L (C) - (F) Reaction condition: [PMS]=5 mmol/L, T = 25 °C, pH = 6. Other chemical reagents used: [FeAlg-ACF] = 2 g/L, [azophloxine] = 50 μmol/L.

2.4. comparison between FeCit@ACFs/PMS/visible light and FeAlg@ACFs/ PMS /visible light system

The Fe(III)-carboxylate complex, FeCit@ACFs/PMS/visible light, had been tested for degradation under the same.The system can degrade azophloxine within 33 minutes, while our catalytic oxidation system, FeCit@ACFs/PMS/visible light, in the same conditions can degrade azophloxine within 21 minutes, and the reusability is stronger.

To further assess the difference in catalytic oxidation activity of these two systems, we adopted a general pseudo-first-order kinetic model ($\ln(C_t/C_0)/k_{obs}t$). As shown in Fig. 4, the kobs for FeAlg-ACFs/PMS/visible light was calculated to be 0.19694 min^{-1}, which was almost 2 fold higher than that for FeCit-ACFs/PMS/visible light (0.1098 min^{-1}).

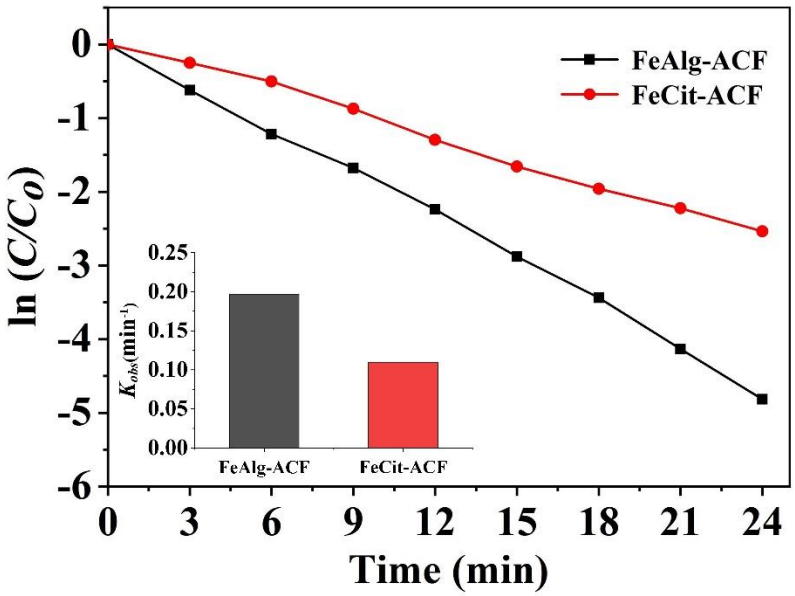

Figure 4. Time profiles of azophloxine decolorization in FeAlg-ACFs/PMS/visible light and FeCit-ACFs/PMS/visible light; the inset shows the kobs of corresponding systems. Reaction condition: [PMS]=5 mmol/L, T = 25 °C, pH = 6. Other chemical reagents used: [FeAlg-ACF] = 2 g/L, [FeCit-ACF] = 2 g/L ,[azophloxine] = 50 μmol/L.

2.5. Reaction kinetics of catalytic oxidation by FeAlg-ACF/PMS system

Two models: pseudo-first-order, pseudo-second-order were used to investigate the degradation kinetics of azophloxine degradation by FeAlg-ACFs/PMS system. Pseudo-first-order model was first described by Lagergren (1898) and can be generally expressed as follows:

$$log(q_e - q_t) = logq_e - k_1 t / 2.303 \quad (10)$$

where q_t is the amount of azophloxine removed at a time t (min) and k_1 is the equilibrium rate constant (min^{-1}). The values of log ($q_e - q_t$) are linearly with t, while k_1 and q_e can be determined from the slope and intercept of the plot of log ($q_e - q_t$) versus t, respectively.

Pseudo-second-order model, known as Ho's pseudo-second-order model, was also applied to analyze the degradation kinetics of azophloxine by using the equation below:

$$t/q_t = 1/(k_2 q_e^2) + t/q_e \quad (11)$$

where k_2 is the rate constant of second order degradation (g mg^{-1} min^{-1}) and $k_2q^2_e$ is the initial degradation rate constant (h). The plot of t/q_t versus t should exhibit a linear relationship, q_e and k_2 can be determined from the slope and intercept of the plot, respectively.

These models were tested for the degradation of azophloxine and the best model was selected depending on the linear regression correlation coefficient, r^2. Table 2 shows the parameters of these degradation kinetic models. The pseudo-first order kinetic model is: -ln (C_t/C_0) = -0.19694t - 0.04125, R^2 is 0.99524, while the pseudo-second-order kinetic model is: $1/C_t$ = -0.09478t - 21.84025, R^2 is 0.98076. We can conclude that the pseudo-second-order model is not suitable for the degradation of azophloxine by FeAlg-ACFs/PMS system because of their relatively low r^2 values. The experimental data fit well with the pseudo-first-order model with $r^2 > 0.99$.

Preprints (www.preprints.org) | NOT PEER-REVIEWED | Posted: 7 January 2020 doi:10.20944/preprints202001.0056.v1

Peer-reviewed version available at Catalysts 2020, 10, 138; doi:10.3390/catal10010138

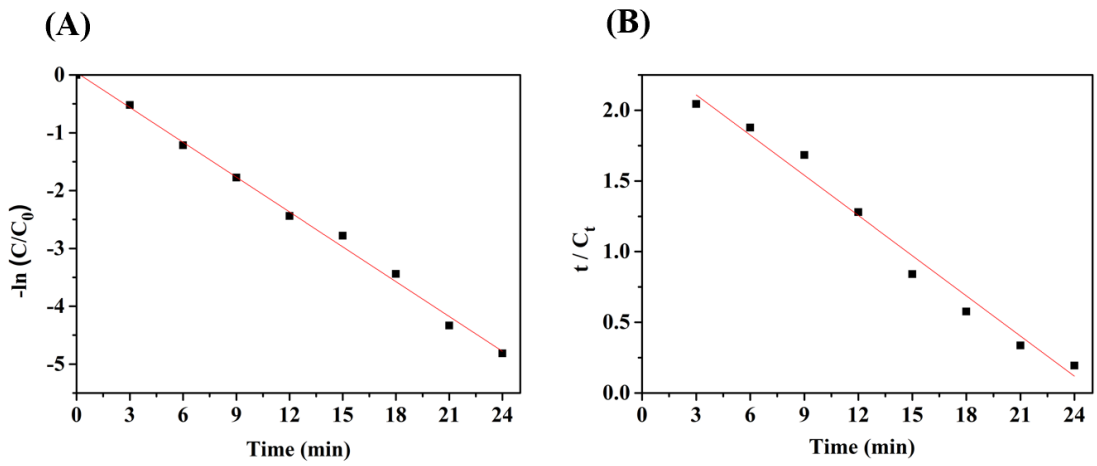

Figure 5. Pseudo-first-order kinetic fitting and pseudo-secondary kinetics fitting of azophloxine degradation. Reaction condition: [PMS]=5 mmol/L, T = 25 °C, pH = 6. Other chemical reagents used: [FeAlg-ACF] = 2 g/L, [azophloxine] = 50 μmol/L.

To better analyze the degradation rate of azophloxine, in-depth research on the theoretical study of the degradation of the target pollutant azophloxine by the reaction system was conducted. Pseudo-first-order dynamics fitting and pseudo-secondary dynamics fitting were performed on azophloxine within 24 min. The fitting results were presented in Fig. 5, and the fitting kinetic constants were illustrated in Table 1.

dye	Dynamic equation series	The fitted reaction rate equation	k_{obs}	Adj.R-Square
azophloxine	pseudo-first order kinetic model	$-\ln(C_t/C_0)=-0.19694t-0.04125$	0.19694	0.99524
	pseudo-second order kinetic model	$1/C_t=-0.09478t-21.84025$	0.09478	0.98076

Table 1. kinetic constants of azophloxine degradation by FeAlg-ACFs/PMS/visible light system

According to azophloxine dye degradation condition, the dynamic test data of kinetics of primary and secondary fitting, it can be seen that FeAlg-ACFs/PMS system oxidative degradation azophloxine of the first-order kinetics reaction of correlation coefficient is greater than the secondary dynamic correlation coefficient, show that the dye degradation process is in line with first-order kinetics reaction process. The degradation rate constant (k_{obs}) of azophloxine was 0.19694.

Applying the principle of chemical kinetics to the field of environment, not only the mechanism of pollutant degradation can be studied, but also the influencing factors of pollutant degradation and stabilization measures can be developed.

2.6. Mechanism of catalytic oxidation by FeAlg-ACF/PMS system

The oxidation of organic pollutants was mainly contributed by ROS generated from PMS oxidation. In this study, we used t-butanol (TBA) and methanol (MA) to study the variation of ROS in the reaction system because MA is highly reactive with $SO4^{\bullet-}$ and •OH, while TBA only shows high reactivity with •OH [59,60].

As shown in Fig. 6A, when 0.5 M TBA was added into our catalytic degradation system, the overall removal ratio of azophloxine dropped sharply from 100% to 42.3%. Therefore, •OH plays an important role in the photocatalytic oxidation reaction. Furthermore, when 0.5 M MA was added into the catalytic system, the removal rate was declined to 26.8%. It was suggested that the inhibition of MA on azophloxine removal was more significant than that of TBA because MA was highly reactive

Preprints (www.preprints.org) | NOT PEER-REVIEWED | Posted: 7 January 2020 doi:10.20944/preprints202001.0056.v1

Peer-reviewed version available at Catalysts 2020, 10, 138; doi:10.3390/catal10010138

with both •OH and SO4•−. Considering the possible influence of competitive adsorption, we further supplemented the free radical capture experiment under dark reaction, as shown in Fig. 6B. As shown in the figure, it can be observed that the overall effect under dark reaction was worse than that under light reaction, and the degradation rate of MA and TBA was further reduced, proved that both •OH and SO4•− were essentially important for the catalytic degradation of azophloxine. The reaction process of PMS activation is shown in Eqs. (12) – (15).

$$M^{2+} + HSO_5^- \rightarrow M^{3+} + SO_4^{\bullet-} + OH^- \quad (12)$$

$$SO_4^{\bullet-} + OH^- \rightarrow SO_4^{2-} + \bullet OH \quad (13)$$

$$M^{3+} + HSO_5^- \rightarrow M^{2+} + SO_5^{\bullet-} + H_2O \quad (14)$$

$$SO_5^{\bullet-} + O_2^- \rightarrow SO_4^{\bullet-} + O_2 \quad (15)$$

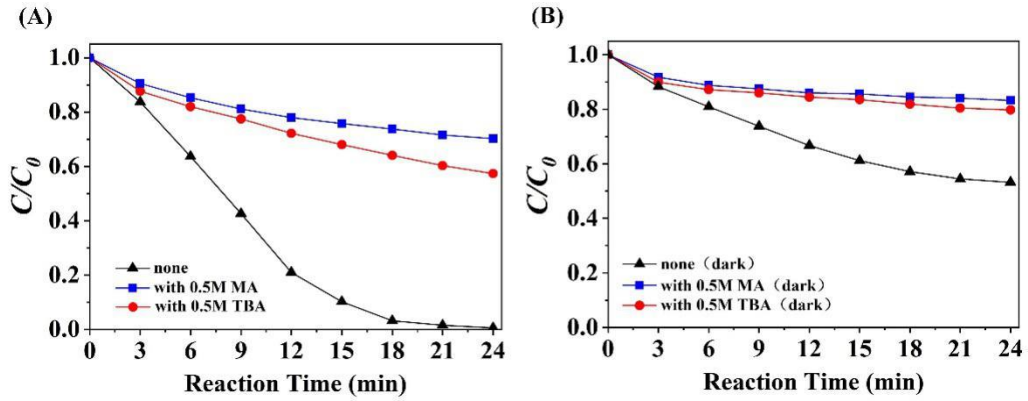

Figure 6. Effects of TBA and MA on the azophloxine removal by FeAlg-ACF/PMS system:(A) with light irradiation. (B) without light irradiation. Reaction conditions: [FeAlg-ACF] = 2 g/L, [PMS] = 5 mmol/L, [azophloxine] = 50 μmol/L, initial pH = 6.0, T = 25℃.

To further understand the mechanism of ACF in the catalytic degradation system, we performed X-ray photoelectron spectroscopy analysis and determined the structural changes of FeAlg-ACF after the reaction. The peaks at 531.6 eV and 533.1 eV correspond to the oxygen atoms in the carbonyl group (C=O) and hydroxyl group (-O-H), respectively. As shown in Fig. 7, the peak strength of oxygen in the C-O-H group decreased after the catalytic degradation of azophloxine. By contrast, the peak strength of oxygen proportionally increased in the C=O bond. It was suggested that C-O-H groups were transformed into C=O during the azophloxine removal. This change confirmed that PFRs in ACF supplied electrons to Fe(III)-Alg, and electron transfer accelerated the Fe(III) to Fe(II) reduction process, which was the key step in accelerating Fenton-like reaction.

In conclusion, we propose a mechanism to explain the azophloxine removal by FeAlg-ACF/PMS system. First, the PFRs in ACF, as electronic storage, provides electrons to the Fe-Alg complex, which accelerates the LMCT process. At the same time, due to the high photosensitivity of Fe-Alg complex, visible light radiation further enhances the LMCT process. Therefore, as a distinctive heterogeneous photocatalyst, FeAlg-ACF can effectively activate PMS to produce •OH and $SO_4^{\bullet-}$ to degrade organic dyes rapidly under visible light.

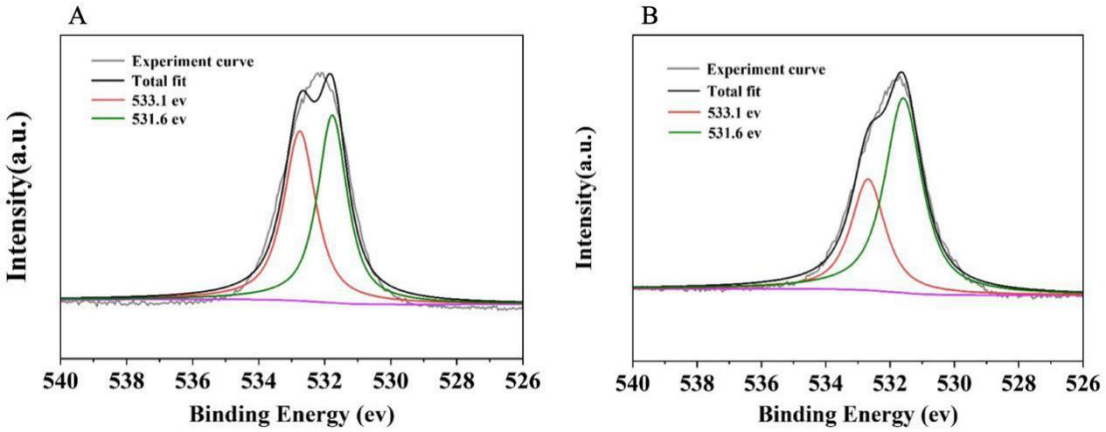

Figure 7. XPS spectra of O1s in FeAlg-ACF before (A) and after (B) its utilization in the FeAlg-ACF/PMS/visible light system. Reaction conditions: [FeAlg-ACF] = 2 g/L, [PMS] = 5 mmol/L, [azophloxine] = 50 μmol/L, initial pH = 6.0, T = 25 ℃.

3. Experimental

3.1. Materials

Activated carbon fiber (ACF) was purchased from Jiangsu Sutong Carbon Fiber Co., Ltd. (Jiangsu, China). $FeCl_3 \cdot 6H_2O$ with analytical pure and sodium alginate $(C_6H_7NaO_6)_n$ with chemical pure were obtained from Sinopharm Chemical Reagent Co., Ltd. (Shanghai, China). Peroxymonosulfate (PMS) with analytical pure was provided by Aladdin biological technology Co., Ltd. (Shanghai, China). Azophloxine (analytical pure) was purchased from Macklin Biochemical Co., Ltd. (Shanghai, China). Rhodamine B (analytical pure), acid orange 7 (analytical pure) and methylene blue (analytical pure) were supplied by Sinopharm Chemical Reagent Co., Ltd. We used ultrapure water throughout the experiment.

3.2. Sample preparation

The preparation scheme of the FeAlg-ACF catalyst is shown in Fig. 8. A certain amount of ACFs (10 g) was soaked in 3 mol/L nitric acid solution, heated in the water bath at 30 ℃ for 12 h. The acidified ACF was repeatedly rinsed by ultrapure water and then was dried in a vacuum drying oven (Shanghai Yiheng Scientific Instrument Co., Ltd., DZF-6020) at 30 ℃. Ferric chloride and sodium alginate were prepared into a suspension of ferric alginate at a 1:1 mass ratio with the ultrasonic stirring method. The acidified ACF was then immersed in the ferric alginate solution at 25 ℃ for 24 hours. After rinsed by ultrapure water and dried at 30 ℃, a novel heterogeneous catalyst FeAlg-ACF will be fulfilled.

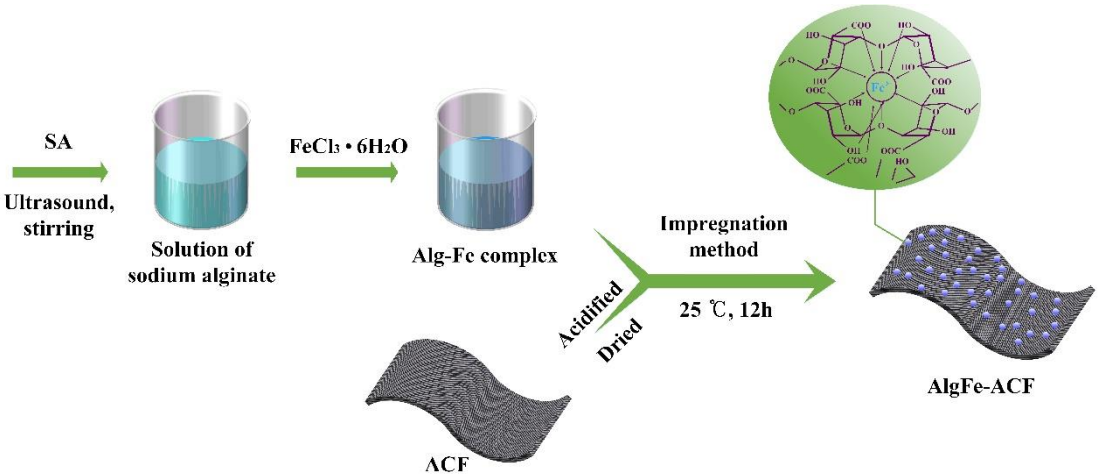

Figure 8. Schematic diagram of preparation process of the heterogeneous photocatalysis FeAlg-ACF.

3.3. Dye removal by FeAlg-ACF

The photocatalytic degradation of azophloxine was conducted in a photochemical reaction apparatus (Shanghai Yuncao, YCYN-GHX-D, Shanghai, China), equipped with a 500 W mercury lamp which irradiated the dyes at a distance of 10 cm through an ultraviolet glass cut-off filter (400 nm). The temperature was kept at 25 ℃ throughout the reaction. The reaction system was composed of azophloxine with the initial concentration of 50 μmol/L, FeAlg-ACF with the dosage of 2 g/L and PMS with initial content of 5 mmol/L. NaOH or HCl solutions were used to adjust the initial pH values of the reaction system. The reaction system was treated in dark for 6 min, followed by photocatalytic degradation with a time interval of 3 min. The absorbance of azophloxine was determined by a UV-visible spectrophotometer (Shimadzu, UV-2550) at a maximum wavelength of 531 nm. According to the change of the absorption value of the sample before and after the reaction, the removal ratio (v) was calculated according to the absorbance of the solution before and after the treatment, using the following equation:

$$v = C_t / C_0 \times 100\% = A_t / A_0 \times 100\% \quad (16)$$

Where C_0 is the initial concentration of azophloxine, C_t is the azophloxine concentration after reaction time t, A_0 is used to show the initial absorbance of azophloxine, A_t is the absorbance of azophloxine after the reaction time [51-53].

3.4. Characterizations

The surface morphologies of the prepared catalyst were observed by scanning electron microscopy (ZEISS Sigma 500/VP Field emission scanning electron microscope). The iron content of the solution after the formation of FeAlg-ACF was determined by PANalytical X-ray fluorescence spectrometry (DY1040). The binding site of O1s was determined by X-ray photoelectron spectroscopy (XPS, Kratos Axis Ultra DLD, Kratos Analytical, Manchester, UK). The binding energy peaks of all XPS spectra were calibrated by using the binding energy peaks of 284.7 eV for principal C1s. The total organic carbon content of the dye solution was measured by a total organic carbon analyzer (Analytik Jena AG, model 3100) and the nitrate concentration was detected by ion chromatography (Thermo Fisher Scientific, Aquion). Characteristic peaks of the reaction solution were explored by LC 3000 high-performance liquid chromatography (Beijing Tong Heng Innovation Technology Co., Ltd., LC 3000).

4. Conclusion

In summary, we fabricated a novel heterogeneous catalyst FeAlg-ACF via a single-step process, i.e. impregnation method. Together with PMS and visible light, we constructed a visible-light photocatalytic degradation system to remove azophloxine from aqueous solution. Azophloxine was completely removed after only 24 min processing by this novel system. In addition, results indicated that more than 93.5% azophloxine has been completely degraded into inorganic compounds, thus potential secondary contamination by intermediate products during catalytic degradation can be inhibited. Compared to iron alginate gel beads, the removal efficiency of dyes was improved by the large specific surface area and PFRs provided by carrier ACF. Moreover, the prepared heterogeneous catalyst FeAlg-ACF exhibits the advantages of reusability, a wide range of pH applications (2 - 10) and availability in visible light. With the additional advantage of recycled usage and ion applicability, the proposed FeAlg-ACF/PMS system is potentially applied in efficiently and environmental-friendly removal of dyeing wastewater.

Acknowledgments: The author would like to thank the Ocean College Experimental Teaching Center of Zhejiang University for SEM characterization, and State Key Laboratory of Silicon

Materials of Zhejiang University for XPS characterization. The authors also thank Lu et al.in department of chemistry, Zhejiang University for helpful discussions and assistance in experiments.

References:

[1] S. Sakaue, T. Tsubakino, Y. Nishiyama, Y. Ishii, J. Org. Oxidation of aromatic amines with hydrogen peroxide catalyzed by cetylpyridinium heteropolyoxometalates. Chem 1993, 58, 3633-3638.
[2] C. Dong, J. Lu, B. Qiu, B. Shen, M. Xing, J. Zhang. Developing stretchable and graphene-oxide-based hydrogel for the removal of organic pollutants and metal ions. Appl. Catal. B: Environ 2018, 222, 146-156.
[3] M. Ahmad, M. Yousaf, A. Nasir, I.A. Bhatti, A. Mahmood, X. Fang, X. Jian, K. Kalantar-Zadeh, N. Mahmood. Porous eleocharis@ MnPE layered hybrid for synergistic adsorption and catalytic biodegradation of toxic Azo dyes from industrial wastewater. Environ. Sci. Technol 2019, 53 2161-2170.
[4] Q. Wang, L. Huang, X. Quan. Sequential anaerobic and electro-Fenton processes mediated by W and Mo oxides for degradation/mineralization of azo dye methyl orange in photo assisted microbial fuel cells. Appl. Catal. B: Environ 2019, 245, 672-680.
[5] P. Shukla, S. Wang, H. Sun, H. Ang, M. Tade. Adsorption and heterogeneous advanced oxidation of phenolic contaminants using Fe loaded mesoporous SBA-15 and H_2O_2. Chem. Eng. J 2010, 164, 255-260.
[6] W. Luo, L. Zhu, N. Wang, H. Tang, M. Cao, Y. She. Efficient removal of organic pollutants with magnetic nanoscaled BiFeO3 as a reusable heterogeneous Fenton-like catalyst. Environ. Sci. Technol 2020, 44, 1786-1791.
[7] C. Gao, S. Chen, X. Quan, Y. Hong, Z. Yao. Enhanced Fenton-like catalysis by iron-based metal organic frameworks for degradation of organic pollutants. J. Catal 2017, 356, 125-132.
[8] X. Yang, X. Xu, J. Xu, Y. Han. Iron oxychloride (FeOCl): an efficient Fenton-like catalyst for producing hydroxyl radicals in degradation of organic contaminants. J. Am. Chem. Soc 2013, 135, 16058-16061.
[9] B. Huang, C.Y. Qi, Z. Yang, Q. Guo, W.Q. Chen, G.M. Zeng, C. Lei. Pd/Fe_3O_4 nanocatalysts for highly effective and simultaneous removal of humic acids and Cr (VI) by electro-Fenton with H2O2in situ electro-generated on the catalyst surface. J. Catal 2017, 352, 337-350.
[10] P.T. Lachkov, Y.H. Chin, Catalytic consequences of reactive oxygen species during C_3H_6 oxidation on Ag clusters. J. Catal 2018, 366, 127-138.
[11] J. Wang, Z. Liu, R. Cai. A new role for Fe3+ in TiO_2 hydrosol: accelerated photodegradation of dyes under visible light. Environ. Sci. Technol 2008, 42, 5759-5764.
[12] W. He, H. Jia, D. Yang, P. Xiao, X. Fan, Z. Zheng, H. Kim, W.G. Wamer, J. Yin. Composition directed generation of reactive oxygen species in irradiated mixed metal sulfides correlated with their photocatalytic activities. ACS. Appl. Mater. Inter 2015, 7, 16440-16449.
[13] K. Song, M. Lu, S. Xu, C. Chen, Y. Zhan, D. Li, C. Au, L. Jiang, K. Tomishige. Effect of alloy composition on catalytic performance and coke-resistance property of Ni-Cu/Mg (Al) O catalysts for dry reforming of methane. Appl. Catal. B: Environ 2018, 239, 324-333.
[14] B. Zhang, Y. Zhang, Y. Teng. Electrospun magnetic cobalt–carbon nanofiber composites with axis-sheath structure for efficient peroxymonosulfate activation. Appl. Surf. Sci 2018, 452, 443-450.
[15] J. Luo, Y. Wang, D. Cao, K. Xiao, T. Guo, X. Zhao. Enhanced photoelectrocatalytic degradation of 2, 4-dichlorophenol by TiO2/Ru-IrO2 bifacial electrode. Chem. Eng. J 2018, 343, 69-77.
[16] S. Liu, X. Zhao, Y. Wang, H. Shao, M. Qiao, Y. Wang, S. Zhao. Peroxymonosulfate enhanced photoelectrocatalytic degradation of phenol activated by Co_3O_4 loaded carbon fiber cathode. J. Catal 2017, 355, 167-175.
[17] Z. Fan, Z. Wang, J. Shi, C. Gao, G. Gao, B. Wang, Y. Wang, X. Chen, C. He, C. Niu. Charge-redistribution-induced new active sites on (0 0 1) facets of α-Mn_2O_3 for significantly enhanced selective catalytic reduction of NOx by NH3. J. Catal 2019, 370, 30-37.

[18] L. Luo, D. Wu, D. Dai, Z. Yang, L. Chen, Q. Liu, J. He, Y. Yao. Synergistic effects of persistent free radicals and visible radiation on peroxymonosulfate activation by ferric citrate for the decomposition of organic contaminants. Appl. Catal. B: Environ 2017, 205, 404-411.
[19] X.N. Wang, W.B. Dong, M. Brigante, G. Mailhot. C_{60} Fullerol Promoted Fe (III)/H_2O_2 Fenton Oxidation: Role of Photosensitive Fe (III)-Fullerol Complex. Appl. Catal. B: Environ 2019, 245, 271-278.
[20] A. Rastogi, S.R. Al-Abed, D.D. Dionysiou. Effect of inorganic, synthetic and naturally occurring chelating agents on Fe (II) mediated advanced oxidation of chlorophenols. Water Res 2009, 43, 684-694.
[21] L. Ling, D.P. Zhang, J.Y. Fang, C.H. Fan, C. Shang. A novel Fe (II)/citrate/UV/peroxymonosulfate process for micropollutant degradation: Optimization by response surface methodology and effects of water matrices. Chemosphere 2017, 184, 417-428.
[22] D.H. Han, J.Q. Wan, Y.W. Ma, Y. Wang, Y. Li, D.Y. Li, Z.Y. Guan, New insights into the role of organic chelating agents in Fe (II) activated persulfate processes. Chem. Eng. J 2015, 269, 425-433.
[23] Z. Xu, G. Gao, B. Pan, W. Zhang, L. Lv. A new combined process for efficient removal of Cu (II) organic complexes from wastewater: Fe (III) displacement/UV degradation/alkaline precipitation. Water Res 2015, 87, 378-384.
[24] Z. Wang, X. Chen, H. Ji, W. Ma, C. Chen, J. Zhao. Photochemical cycling of iron mediated by dicarboxylates: special effect of malonate. Environ. Sci. Technol 2010. 44, 263-268.
[25] H. Pang, Q. Zhang, H. Wang, D. Cai, Y. Ma, L. Li, K. Li, X. Lu, H. Chen, X. Yang, J. Chen. Photochemical Aging of Guaiacol by Fe (III)–Oxalate Complexes in Atmospheric Aqueous Phase. Environ. Sci. Technol 2019, 53, 127-136.
[26] J. Chen, W.R. Browne, Coord. Photochemistry of iron complexes. Chem. Rev2018, 374, 15-35.
[27] C. Ruales-Lonfat, J.F. Barona, A. Sienkiewicz, J. Vélez, L.N. Benítez, C. Pulgarín. Bacterial inactivation with iron citrate complex: a new source of dissolved iron in solar photo-Fenton process at near-neutral and alkaline pH. Appl. Catal. B: Environ 2016, 180, 379-390.
[28] L. Li, Y. Fang, R. Vreeker, I. Appelqvist, E. Mendes. Reexamining the egg-box model in calcium–alginate gels with X-ray diffraction. Biomacro 2007, 8, 464-468.
[29] Y. Dong, W. Dong, Y. Cao, Z. Han, Z. Ding. Preparation and catalytic activity of Fe alginate gel beads for oxidative degradation of azo dyes under visible light irradiation. Today 2011. 175, 346-355.
[30] J. Fernandez, M.R. Dhananjeyan, J. Kiwi, Y. Senuma, J. Hilborn. Evidence for Fenton photoassisted processes mediated by encapsulated Fe ions at biocompatible pH values. J. Phys. Chem. B 2000, 104, 5298-5301.
[31] B. Li, Y. Dong, C. Zou, Y. Xu. Iron (III)–alginate fiber complex as a highly effective and stable heterogeneous fenton photocatalyst for mineralization of organic dye. Ind. Eng. Chem. Res 2014, 53, 4199-4206.
[32] R.P. Narayanan, G. Melman, N.J. Letourneau, N.L. Mendelson, A. Melman. Photodegradable iron (III) cross-linked alginate gels. Biomacro 2012, 13, 2465-2471.
[33] H. Titouhi, J.E. Belgaied. Removal of ofloxacin antibiotic using heterogeneous Fenton process over modified alginate beads. J. Environ. Sci. (China) 2016, 45, 84-93.
[34] O. Iglesias, J. Gómez, M. Pazos, M.Á. Sanromán. Electro-fenton oxidation of imidacloprid by fe alginate gel beads. Appl. Catal. B: Environ 2014, 144, 416-424.
[35] W.F. Zhang, F. Liu, Y.G. Sun, J. Zhang, Z.P. Hao. Simultaneous redox conversion and sequestration of chromate (VI) and arsenite (III) by iron (III)-alginate based photocatalysis. Appl. Catal. B: Environ 2019, 259, 118046.
[36] X. Tao, J. Su, L. Wang. A new heterogeneous catalytic system for wastewater treatment: Fe-immobilized polyelectrolyte microshells for accumulation and visible light-assisted photooxidative degradation of dye pollutants. J. Mol. Catal. A-Chem 2008, 280, 186-193.
[37] S. Lim, Y. Zheng, S. Zou, J.P. Chen. Characterization of copper adsorption onto an alginate encapsulated magnetic sorbent by a combined FT-IR, XPS, and mathematical modeling study. Environ. Sci. Technol 2008, 42, 2551-2556.
[38] R. Gonzalez-Olmos, M.J. Martin, A. Georgi, F.D. Kopinke, I. Oller, S. Malato. Fe-zeolites as

heterogeneous catalysts in solar fenton-like reactions at neutral ph. Appl. Catal. B: Environ 2012, 125, 51-58.
[39] H.W. Ji, W.J. Song, C. Chen, H. Yuan, W. Ma, J. Zhao. Anchored oxygen-donor coordination to iron for photodegradation of organic pollutants. Environ. Sci. Technol 2007, 41, 5103-5107.
[40] M. Cheng, W.H. Ma, C. Chen, J. Yao, J. Zhao. Photocatalytic degradation of organic pollutants catalyzed by layered iron(ii) bipyridine complex–clay hybrid under visible irradiation. Appl. Catal. B: Environ 2006, 65, 217-226.
[41] J.Y. Feng, X.J. Hu, P.L. Yue. Novel bentonite clay-based Fe− nanocomposite as a heterogeneous catalyst for photo-fenton discoloration and mineralization of orange II. Environ. Sci. Technol 2004, 38, 269-275.
[42] F. Duarte, F.J. Maldonado-Hódar, L.M. Madeira. Prussian blue onto activated carbon as a catalyst for heterogeneous fenton-like processes. Appl. Catal. B: Environ 2013, 129, 264-272.
[43] S. Yang, X. Yang, X. Shao, R. Niu, L. Wang. Activated carbon catalyzed persulfate oxidation of Azo dye acid orange 7 at ambient temperature. J. Hazard. Mater 2011, 186, 659-666.
[44] L. Hu, X. Yang, S. Dang. An easily recyclable Co/SBA-15 catalyst: heterogeneous activation of peroxymonosulfate for the degradation of phenol in water. Appl. Catal. B: Environ 2011, 102, 19-26.
[45] Y. Huang, L. Peng, Y. Liu, G. Zhao, J.Y. Chen, G. Yu. Biobased nano porous active carbon fibers for high-performance supercapacitors. ACS. Appl. Mater. Inter 2016, 8, 15205-15215.
[46] J.M. Valente Nabais, P.J.M. Carrott. Chemical characterization of activated carbon fibers and activated carbons. J. Chem. Educ 2006, 83, 436.
[47] Y. Yao, L. Wang, L. Sun, S. Zhu, Z. Huang, Y. Mao, W. Lu, W. Chen. Efficient removal of dyes using heterogeneous Fenton catalysts based on activated carbon fibers with enhanced activity. Chem. Eng. Sci 2013, 101, 424-431.
[48] Y. Zhang, Y. Tang, Q. Qiu, Y. Chen, Y. Sun, P. Wan, X.J. Yang. Electrochemically Enhanced Adsorption of Aluminum from Sodium Carbonate Solution by Activated Carbon Fibers. Ind. Eng. Chem. Res 2013, 52, 14449-14455.
[49] B. Zhang, Y. Zhang, Y. Teng. Electrospun magnetic cobalt–carbon nanofiber composites with axis-sheath structure for efficient peroxymonosulfate activation. Appl. Surf. Sci 2018, 452, 443-450.
[50] H.Y. Li, N.J. Li, D.Y. Chen. Polyethylene imine-grafted ACF@ BiOI0. 5Cl0. 5 as a recyclable photocatalyst for high-efficient dye removal by adsorption-combined degradation. Appl. Surf. Sci 2017, 403, 80-88.
[51] A. Cihanoğ lu, G. Gündüz, M. Dükkancı. Degradation of acetic acid by heterogeneous Fenton-like oxidation over iron-containing ZSM-5 zeolites. Appl. Catal. B: Environ 2015, 165, 687-699.
[52] R. Gonzalez-Olmos, M.J. Martin, A. Georgi, F. Kopinke, I. Oller, S. Malato. Fe-zeolites as heterogeneous catalysts in solar fenton-like reactions at neutral ph. Appl. Catal. B: Environ 2012, 125, 51-58.
[53] M. Aleksić, H. Kušić, N. Koprivanac, D. Leszczynska, A.L. Božić. Heterogeneous Fenton type processes for the degradation of organic dye pollutant in water-The application of zeolite assisted AOPs. Desalination 2010, 257, 22-29.
[54] R. Gonzalez-Olmos, F.D. Kopinke, K. Mackenzie. Hydrophobic Fe-zeolites for removal of MTBE from water by combination of adsorption and oxidation. Environ. Sci. Technol 2013, 47, 2353-2360.
[55] Z.Q. Zeng, H.K. Zou, X. Li, M. Arowo, B.C. Sun, J.F. Chen, G.W. Chu, L. Shao. Degradation of phenol by ozone in the presence of Fenton reagent in a rotating packed bed. Chem. Eng. J 2013, 229, 404-411.
[56] C. Duesterberg, S. Mylon, T. Waite. PH effects on iron-catalyzed oxidation using Fenton's reagent. Environ. Sci. Technol 2008, 42, 8522-8527.
[57] X. Chen, W.H. Ma, J. Li, Z.H. Wang, C. Chen, H.W Ji, J.C. Zhao. Photocatalytic oxidation of organic pollutants catalyzed by an iron complex at biocompatible pH values: using O_2 as main oxidant in a Fenton-like reaction. J. Phys. Chem. C 2011, 115, 4089-4095.
[58] M. Cuartero, G. Crespo, T. Cherubini, N. Pankratova, F. Confalonieri, F. Massa, M. Tercier-Waeber, M. Abdou, J. Schäfer, E. Bakker. In situ detection of macronutrients and chloride in seawater by submersible electrochemical sensors. Anal. Chem 2018, 90, 4702-4710.

[59] H.D. Xu, D. Wang, J. Ma, T. Zhang, X.H. Lu, Z.Q. Chen. A superior active and stable spinel sulfide for catalytic peroxymonosulfate oxidation of bisphenol S. Appl. Catal. B: Environ 2018, 238, 557-567.
[60] S.E. Page, M. Sander, W.A. Arnold, K. McNeill. Hydroxyl radical formation upon oxidation of reduced humic acids by oxygen in the dark. Environ. Sci. Technol 2012, 46, 1590-1597.